

Reduction Kinetics of Ag_2MoO_4 by Hydrogen

J.C. JUAREZ and R. MORALES

Ag_2O and MoO_3 powders were mechanically (ball) milled with the objective of obtaining a Ag_2MoO_4 phase for subsequent reduction with hydrogen gas. A thermogravimetric unit was used to follow the course of the reduction process aiming at the chemical reaction as the rate controlling step. Isothermal reduction experiments were performed on the individual oxides to establish a ground for the reduction parameters of silver molybdate. Consequently, a nonisothermal treatment was used on Ag_2MoO_4 . It was found that Ag_2MoO_4 is reduced in three steps, *e.g.*, Ag_2MoO_4 to MoO_3 and Ag followed by MoO_3 to MoO_2 and finally MoO_2 to Mo. By assuming a shrinking core model, the calculated activation energies for the first and second reduction steps were 69 and 29 kJ/mol, respectively. While the former value is in good agreement with the activation energy obtained from the isothermal reduction of Ag_2O to Ag, 64 kJ/mol, the latter was found to be lower than the corresponding value for MoO_3 to MoO_2 under isothermal conditions, 124 kJ/mol. It was found that the presence of metallic silver obtained from the initial reduction step of Ag_2MoO_4 not only lowers the energy barrier but the reducing temperature of the subsequent reaction steps (*i.e.*, $\text{MoO}_3 \rightarrow \text{MoO}_2 \rightarrow \text{Mo}$).

DOI: 10.1007/s11663-008-9173-3

© The Minerals, Metals & Materials Society and ASM International 2008

I. INTRODUCTION

HYDROGEN reduction of mixed oxides enables the formation of an alloy containing a low melting metal (*e.g.*, Au) with a high melting metal (*e.g.*, Co). For example, in the reduction of cobalt aluminate (CoAl_2O_4) by hydrogen,^[1] to form cobalt with Al_2O_3 particles, indications were obtained that at temperatures higher than 1273 K, part of the alumina was reduced and the produced aluminum formed a binary Al-Co alloy. Similarly, in the reduction of ZnWO_4 with hydrogen, a new W-Zn phase was obtained.^[2]

The reduction of MoO_3 with hydrogen has been subject of numerous investigations^[3-7] with contrasting opinions on the kinetics of the reduction of MoO_3 to Mo. For example, Hawkins *et al.*^[3] studied the reduction of molybdenum oxide by hydrogen in the temperature range 573 to 723 K and found intermediate suboxides between MoO_2 and MoO. Orehtsky *et al.*^[4,5] separately investigated the kinetics of hydrogen reduction of static powder beds of MoO_3 to MoO_2 and MoO_2 to Mo at temperature ranges of 732 to 877 K and 686 to 1083 K, respectively. The activation energies reported for both processes were approximated to 70 kJ/mol. Arnoldy *et al.*^[6] investigated the reduction of MoO_3 and MoO_2 by varying parameters such as heating rate, sample size, H_2O content of the reducing mixture (H_2/Ar), and precalcination temperature. In this study, the reported activation energy values ranged

from 80 to 405 kJ/mol. Du Sichen and Seetharaman^[7] carefully analyzed the hydrogen reduction of MoO_3 and MoO_2 by using thin pellets of the oxides placed in crucibles with relatively high walls. The activation energies reported by these authors were 211 kJ/mol for the reduction of MoO_3 to MoO_2 and 85 kJ/mol for MoO_2 to Mo. On the other hand, there does not appear to be much information in the literature on the kinetics of the reduction of Ag_2O by hydrogen. This may be due to the fact the Ag_2O starts decomposing at about 473 K. Indeed, the kinetics of the thermal decomposition of Ag_2O has received large attention.^[8]

Silver alloys and silver composites find application as electrical contacts due to their high thermal and electrical conductivity. To ensure high electrical conductivity and strong wear resistance, the properties of silver are combined with those of other materials. Powder metallurgy provides a suitable route for the production of refractory alloys especially when the components of refractory alloys have greatly differing melting temperatures, limited mutual solubility, and different densities. Moreover, the powder metallurgy processing route is highly economically competitive. On the synthesis of Ag-Mo base materials, only one reference has been found, Stolk *et al.*^[9] These authors synthesized Ag-Mo composites by heat treating silver molybdate (Ag_2MoO_4) powders in H_2 atmosphere to address the thermal properties of the product material. Silver and its alloys have excellent electrical, thermal, optical, or catalytic properties. An investigation of the reduction kinetics of silver molybdate would be of considerable value. Thus, the objective of this work is to study the reduction kinetics of Ag_2MoO_4 by hydrogen aiming at the rate of the chemical reaction as the rate controlling step. To obtain the silver molybdate phase, Ag_2O and MoO_3 powders, in stoichiometric ratios, were

J.C. JUAREZ, Researcher, formerly with the Instituto de Investigaciones Metalúrgicas, UMSNH, is with Universidad Autónoma del Estado de Hidalgo, Pachuca 42180, Mexico. R. MORALES, Professor, is with the Instituto de Investigaciones Metalúrgicas, UMSNH, Morelia, Mexico. Contact e-mail: r.morales@umich.mx

Manuscript submitted August 20, 2007.

Article published online September 16, 2008.

ball milled to ensure a uniform distribution of Ag and Mo ions.

II. EXPERIMENTAL

Silver molybdate (Ag_2MoO_4) was prepared at the stoichiometric composition by mixing Ag_2O (99.0 pct Alfa Aesar, Ward Hill, MA) and MoO_3 (99.5 pct Alfa Aesar) powders in required proportions followed by mechanical ball milling using a shaker ball mill (SPEX 8000, Metuchen, NJ). Stainless steel balls were used in the mill, while the ball-to-powder weight ratio was kept to 10:1. The milling process was limited to 5 hours to minimize iron contamination.

Isothermal experiments were carried out on Ag_2O and MoO_3 powders, while nonisothermal experiments were employed on Ag_2MoO_4 . Both types of reduction experiments were carried out using a horizontal thermogravimetric apparatus (Mettler Toledo 581e, Mexico, D.F., Mexico), which has an accuracy of $1 \mu\text{g}$. The balance was controlled by a personal computer through an interface. The weight change during the reduction experiments was recorded by the computer at 1-second intervals. An alumina crucible with 8-mm inner diameter and 1-mm height was used to hold the sample. Typically, about 35 mg of powder were used in each experiment to just form a thin layer. The crucible containing the sample was placed on one end of an alumina rod from the balance. The reactor was made of dense alumina with 16-mm inner diameter. The temperature of the furnace was controlled by a Pt-13 pct Rh/Pt (R-type) thermocouple placed just below the crucible. The fluid flows of the inert gas and reactant gas were individually regulated using mass-flow controllers. Argon and hydrogen gases (99.99 pct) were used in the reduction experiments, which were not further cleaned; however, the influence of the impurities in the hydrogen gas over the reduction kinetics should be well within the limits of experimental error.

In the isothermal experiments, the reaction chamber was flushed with argon gas for 30 minutes after introducing the sample. Then, the sample was heated to the reduction temperature at a heating rate of 25 K/min under a constant flow of argon of 0.1 L/min. Once the reduction temperature was stabilized, the argon gas was stopped and hydrogen gas was introduced into the reaction chamber to start the reduction process. After no more weight loss of the sample was recorded by the computer, the experiment was terminated by cooling the furnace to room temperature at the highest cooling rate (~ 50 K/min). In the case of a nonisothermal experiment, the reaction chamber was initially flushed with hydrogen for 30 minutes after introducing the sample into the furnace. A constant flow of hydrogen gas (0.3 L/min) was maintained throughout the heating cycle. The sample was then heated at a constant heating rate. The experiment was then terminated in a similar fashion as in the case of the isothermal reduction. To eliminate the effect of mass-transfer effect through the powder bed, *i.e.*, gas transport resistance from the bulk stream to the bottom of the crucible, an optimum amount of

powder was determined by examining the reduction rate as a function of the mass sample, which is proportional to the thickness of the powder bed. Moreover, to help focus on the rate of chemical reaction as the controlling step, a hydrogen flow rate of 0.3 L/min was established, as it should be well above the starvation rate for the reduction reactions studied given the small amount of particles used.

The phases of the products obtained after ball milling and hydrogen reduction were identified by X-ray diffraction (XRD) analysis using a Siemens D5000 diffractometer (Mexico, D.F., Mexico) at 30 mA, 50 kV, and 0.02 deg/s step size using $\text{Cu } K_\alpha$ radiation. The particle size distribution of the oxides was determined using a Horiba centrifugal particle analyzer, model CAPA 500 (Irvine, CA).

III. RESULTS

The average particle size for the starting powders, Ag_2O and MoO_3 , and the milled powders were 0.15, 0.69, and $1.2 \mu\text{m}$, respectively. The XRD spectrum of milled powders along with the identified phases are shown in Figure 1. As it can be seen, powders mainly consist of Ag_2MoO_4 with small Bragg peaks of MoO_3 and Ag_2O . The presence of small amounts of MoO_3 and Ag_2O could indicate that the milling time was not sufficient to completely form the Ag_2MoO_4 phase. However, the former two phases should be distributed uniformly within the mixture, which would be favorable for the subsequent reduction process.

To better elucidate the reducing mechanism of Ag_2MoO_4 , isothermal reduction experiments were individually performed on Ag_2O and MoO_3 powders. Figure 2 shows the isothermal reduction curves of Ag_2O by hydrogen at different temperatures. The dimensionless mass change X represents the ratio of the instant mass loss Δm_t to the theoretical final mass

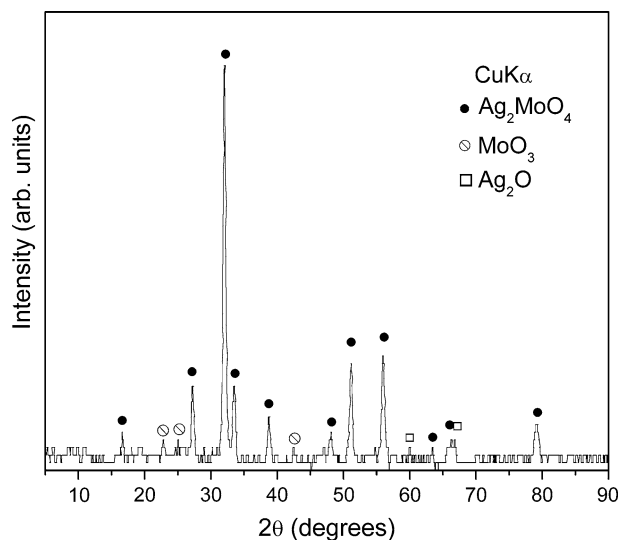


Fig. 1—XRD patterns for Ag_2O - MoO_3 mixture (1:1 molar ratio) after ball milling.

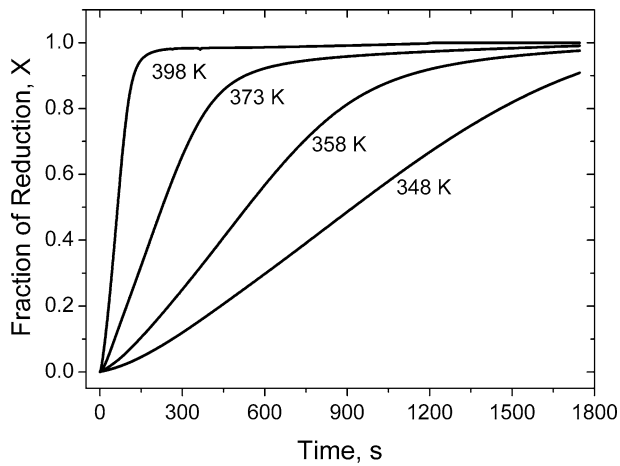


Fig. 2—Isothermal reduction curves of Ag_2O .

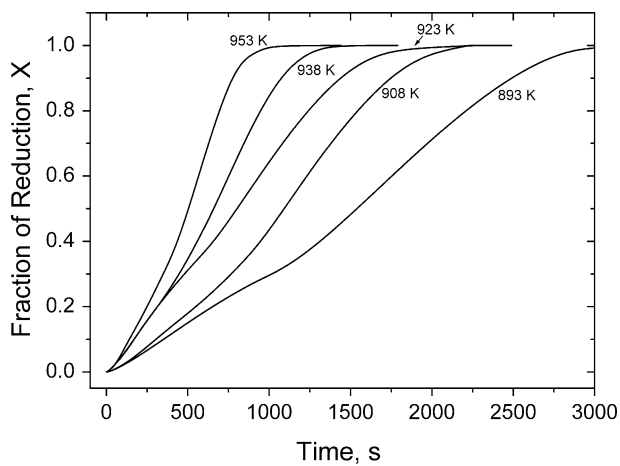


Fig. 3—Isothermal reduction curves of MoO_3 .

loss Δm_∞ , the latter corresponding to the loss of all the oxygen atoms from the oxide. As it can be seen, the reaction rate increases with increasing temperature with a suitable temperature range between 348 and 398 K. Figure 3 shows the reduction rate of MoO_3 by hydrogen as a function of temperature between 893 and 953 K. To avoid uncertainties in the experimental data, the maximum reducing temperature of MoO_3 was limited to 953 K due to the dramatic sublimation of MoO_3 solid occurring at temperatures above 973 K and below the melting point of MoO_3 (1055 ± 5 K). In each reduction curve, a distinct change in the slope is observed in the range $X = 0.2$ to 0.3 . The change in the slope is expected at about $X = 0.3$, as the complete reduction of MoO_3 to MoO_2 should theoretically correspond to $X = 0.33$. To verify the effect of gaseous diffusion between particles on the reaction rate at 923 K, the powder bed height was increased by increasing the weight of the sample from 35 to 50 mg, as shown in Figure 4. As it can be seen, both reduction curves are invariant of the bed height (*i.e.*, sample weight) from the beginning of the process toward the complete reduction

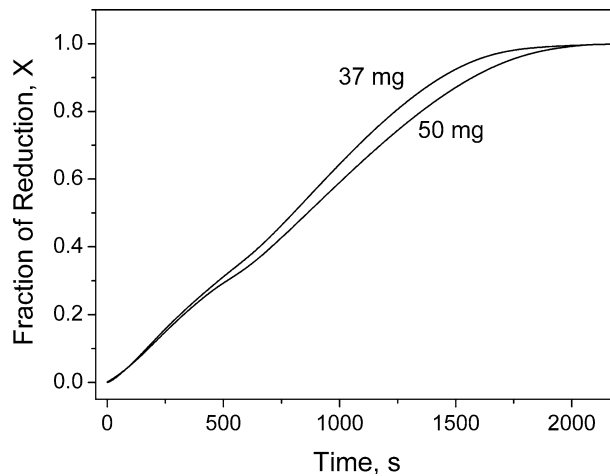


Fig. 4—Effect of powder bed height on the isothermal reduction rate of MoO_3 at 923 K.

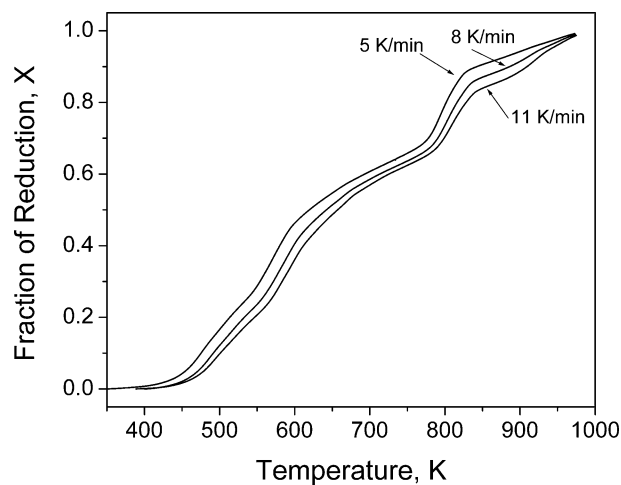


Fig. 5—Nonisothermal reduction curves of Ag_2MoO_4 .

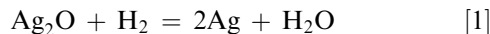
of MoO_3 to MoO_2 ($X = 0.33$). After the complete reduction of MoO_3 to MoO_2 , the reduction curves tend to separate from each other, indicating the dependence of the reaction rate (dX/dt) on the bed height.

Because the temperature range for the reduction of MoO_3 is higher than that for Ag_2O by about 500 K, it was deemed necessary to study the reduction kinetics of Ag_2MoO_4 under nonisothermal conditions, because an isothermal process would require a very wide temperature range that is not suitable for the evaluations of activation energies. Thus, Figure 5 shows the nonisothermal reduction of Ag_2MoO_4 at different scanning rates. As it can be seen, the reduction curves show a similar pattern independent of the heating rate. Distinctive changes in the slopes indicate that the reduction process goes through intermediate steps. The reduction steps toward the completion of the reaction depend on the heating rate, because there is no overlapping of the reduction curves. Toward the end of the process, the reduction rate becomes slower the lower the scanning rate.

IV. DISCUSSION

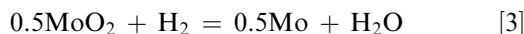
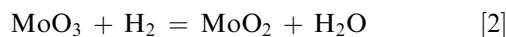
A. Isothermal Reduction

In the present work, the reduction curves of Ag_2O by H_2 show no discontinuities in their slopes, suggesting a one-step process according to the following reaction:



Because the reduction curves shown in Figure 2 clearly indicate that the process is sensitive to temperature, it is logical to assume that the chemical reaction is the rate controlling step under the given experimental conditions.

Figure 3 shows the reduction curves of MoO_3 at different temperatures. It is evident that these curves present a change in slope at about $X = 0.3$ being clearer at lower temperatures. This is an interesting observation as the complete reduction of MoO_3 to MoO_2 should theoretically correspond to $X = 0.33$. Beyond this point, the reduction rate shows a sigmoidal trend for the MoO_2 conversion. While the acceleratory period in the sigmoidal curve indicates the onset of the MoO_2 to Mo conversion, the decaying period would most probably be the result of the diminished reaction surface. Therefore, under the prevailing experimental conditions, the reduction of MoO_3 involves two main reduction steps:



Reaction [2] would be controlled by the rate of chemical reaction, as Figure 4 shows that the slopes of the reduction curves corresponding to $X < 0.3$ are nearly the same. In this case, the gas composition at the internal surface of the particles is quite the same as that in the bulk gas phase. Therefore, gas diffusion between particles does not offer any considerable resistance, and only the chemical reaction offers the major resistance to the reduction process. On the other hand, Reaction [3] is likely to be affected by the rate of mass transport due to the fact that the slopes of the reduction curves for $X > 0.33$ (Figure 4) are relatively different, indicating that gas diffusion between particles proceeds at a slower rate than the rate of chemical reaction. Thus, the resistance caused by the gas diffusion becomes significant.

The existence of suboxide phases during the reduction of MoO_3 with hydrogen has been controversial. For example, Du Sichen and Seetharaman^[7] carried out SEM studies on MoO_3 thin compacts partially reduced by hydrogen at 873 and 973 K. Their studies showed that MoO_2 was the unique intermediate phase during the reduction process, although there exist two intermediate phases such as Mo_9O_{26} and Mo_4O_{11} between MoO_3 and MoO_2 phases, as illustrated in the phase diagram $\text{Mo}-\text{MoO}_3$ constructed by Bygdén *et al.*^[10] Other authors^[11] reported the intermediate phase Mo_4O_{11} before reaching the MoO_2 phase by hydrogen reduction

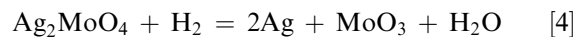
at 823 K. Ressler *et al.*^[12] studied the reduction of MoO_3 with hydrogen in the temperature range from 623 to 823 K and hydrogen concentration from 5 to 100 vol pct. They found that Mo_4O_{11} forms only under certain reaction conditions (H_2 concentration < 20 vol pct and at temperatures above 698 K), where the reduction of MoO_3 is considerably slow that it permits the formation of Mo_4O_{11} . They also reported that the formation Mo_4O_{11} is not an intermediate product during the reduction of MoO_3 but is rather formed in a parallel reaction from MoO_3 and MoO_2 . In the present work, the reduction of MoO_3 proceeds considerably fast due to the higher reducing temperatures employed. Thus, neither Mo_9O_{26} nor Mo_4O_{11} phases were identified by XRD on samples partially reduced.

Similar to Reaction [1], Reaction [2] is likely to be controlled by the rate of the chemical reaction in view of the following facts.

- (1) Sample powders used in this investigation were essentially of a few microns in size; therefore, the thickness of the product layer is small and thus it is not likely to offer any appreciable resistance to the reactant and product gas species.
- (2) The change of the height of the bed, by increasing the sample weight from 35 to 50 mg, had a noticeable effect on the reaction rate only beyond $X = 2$ (Figure 4), implying thereby that the rate of gas diffusion through the powder bed was not mechanism controlling the reduction reaction in the beginning of Reaction [2].
- (3) Under the previous circumstances, using a flow rate of 0.3 L/min, the rate of mass transfer from the bulk of the gas stream to the external surface of the powder bed is not likely to hinder the course of the reaction.
- (4) Given that the amount of the oxide powder used is very small, the impact of the endothermic heat of the reaction on the temperature of the particles could be assumed to be negligible; therefore, the heat-transfer aspect can be ruled out.

B. Nonisothermal Reduction

From the preceding isothermal results, the nonisothermal reduction of Ag_2MoO_4 is first reduced to Ag and MoO_3 according to the following reaction:



Then, continue through Reactions [2] and [3]. This was confirmed by XRD analysis, which revealed Mo and Ag as the unique phases present in the reduced product, as shown in Figure 6. In the reduction of Ag_2MoO_4 , changes in the slopes were more evident. To acquire a deeper understanding of the reduction mechanisms associated with these behaviors, the derivative of X with respect to time, dX/dt , from the nonisothermal reduction curve with a scanning rate of 11 K/min was plotted as a function of temperature along with the

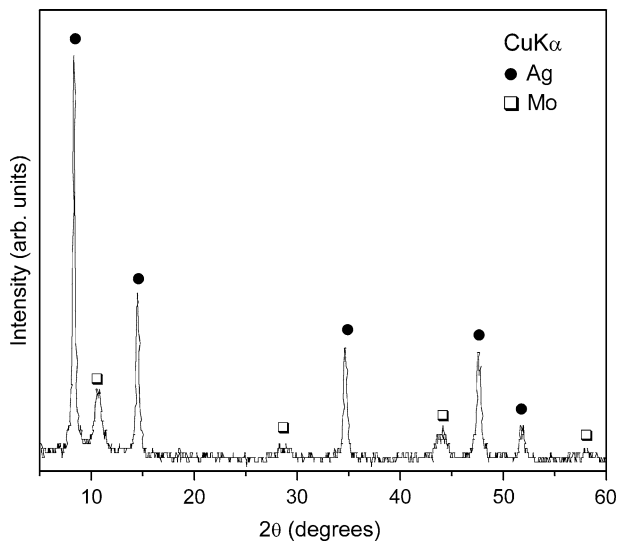


Fig. 6—XRD pattern of the product obtained after the nonisothermal reduction of Ag_2MoO_4 .

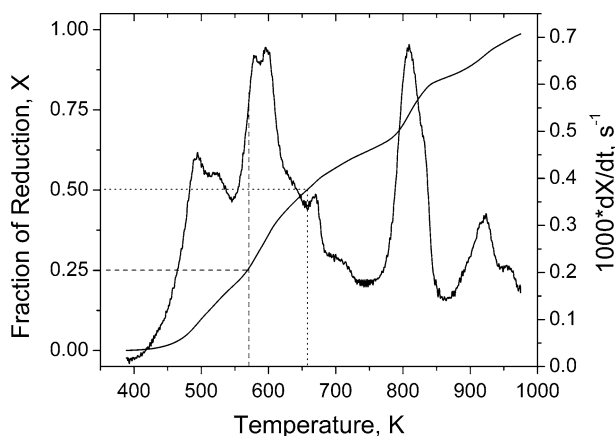
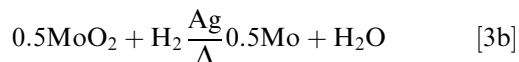
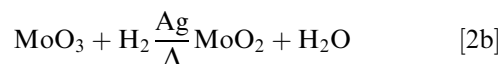


Fig. 7—Differential reduction rate dX/dt against temperature for a nonisothermal experiment at 11 K/min.

corresponding reduction curve, as shown in Figure 7. The dashed lines indicate the theoretical fraction of transition from Reaction [4] to Reaction [2] and Reaction [2] to Reaction [3], $X = 0.25$ and $X = 0.5$, respectively. Figure 7 shows that dX/dt increases and decreases irregularly with increasing temperature. This behavior may be explained as follows. In the region comprising Reaction [4] ($0 < X < 0.25$), the reduction of Ag_2O starts at about 350 K and the reduction rate shows a sharp increase as a consequence of the increase in temperature up to 495 K. This temperature is above the temperature range used in the isothermal reduction of Ag_2O (348 to 398 K). From 495 K, the reduction rate decreases up to 545 K. This decreasing trend could indicate that the reduction mechanism changes from chemical control to mix control, because the rate of chemical reaction increases to the extent where it is no longer the slowest rate step, as established by Szekely *et al.*^[13] and Levenspiel.^[14] Before the

theoretical completion of Reaction [4] ($X \leq 0.25$), dX/dt increases again, indicating that the reduction of MoO_3 to MoO_2 might have been initiated before Ag_2O is completely reduced. In the region comprising Reaction [2] ($0.25 < X < 0.5$), the reduction rate of MoO_3 to MoO_2 increases up to 600 K. Beyond this temperature, dX/dt decreases progressively until the theoretical completion value is reached, $X = 0.5$. It should be noticed that the reduction of MoO_3 to MoO_2 occurs in the temperature range 570 to 650 K, which is significantly lower with respect to the temperature range found in the isothermal reduction of the single oxide (MoO_3), 893 to 953 K. This disparity cannot be explained on the very basis of particle diameter difference between the single and complex oxide but rather on the possible catalytic effect of the free silver content obtained from the preceding reaction. Namely, silver provides a surface with active catalytic sites on which reactants (H_2 and Mo oxides) temporarily become adsorbed and bonds in the reactants become weakened sufficiently for products to be created. The catalyst releases the products without affecting them. This process increases the reaction rate and lower activation energy. While the catalytic effect of silver explains the initial increase in the reaction rate, the subsequent decrease would most probably be due to the diminished reaction surface besides high concentration of H_2O (g) at the reaction interface caused by the fast consumption of H_2 , hindering thus the driving force for the chemical reaction.

In the last step of reduction (MoO_2 to Mo, $X > 0.5$), the reaction rate depicts a sigmoidal trend. This behavior may be caused by the action of opposed driving forces. That is to say, on the one hand, the catalytic effect of silver and the increase in temperature tend to increase the reaction rate, and, on the other hand, the reversible character of Reaction [3] makes the course of the reduction highly sensitive to slight variations of H_2O (g) partial pressure buildup at the reaction interface. To account for the catalytic effect, Reactions [2] and [3] involved in the reduction of Ag_2MoO_4 will be henceforth referred to as



C. Isothermal Kinetics Analysis

To acquire a kinetic characterization of the individual oxides, the shrinking core model was applied to the gas-solid reaction occurring in each individual particle for Reactions [1] and [2] under isothermal conditions. Attempts to apply this model to Reaction [3] were not made, because it was found that mass diffusion affects the reaction mechanism for $X > 0.3$, which corresponds to the reduction of MoO_2 to Mo (Figure 4). Mass diffusion affects the reduction stage from MoO_2 to Mo, because this reaction has a very small equilibrium

constant, which makes the reduction reaction extremely sensitive to mass-transfer rate steps. Thus, if Reactions [1] and [2] are of first order with respect to hydrogen and are irreversible, the relationship between the reaction time, t , and the fraction of reduction, X , for the chemical reaction control can be expressed as^[15]

$$t = \frac{\rho_{\text{oxide}} \cdot r_0}{M_{\text{oxide}} \cdot k \cdot P_{\text{H}_2}} \left[1 - (1 - X)^{1/3} \right] \quad [5]$$

where r_0 is the initial radius of the particle; ρ_{oxide} and M_{oxide} stand for the density and molecular weight of oxide, respectively; k is the reaction rate constant; and P_{H_2} corresponds to the hydrogen partial pressure. Assuming that at given temperature the aforementioned terms remain constant, $[1 - (1 - X)^{1/3}]$ should be a linear function of t if the reduction is controlled by the chemical reaction at the interface between product layer and the unreacted core in each particle. The plots of $[1 - (1 - X)^{1/3}]$ against time at different experimental temperatures for Reactions [1] and [2] are presented in Figures 8 and 9, respectively. All curves showed a correlation coefficient better than 0.99. An activation energy for Reactions [1] and [2] was calculated by combining Eq. [5] with Arrhenius rate law as expressed by the following equation:

$$k = k_o \exp\left(-\frac{Q}{RT}\right) \quad [6]$$

where k_o is a constant, Q is the activation energy of the reaction, T is the temperature in K, and R is the gas constant. The combination of Eqs. [5] and [6] leads to the following expression:

$$\frac{1 - (1 - X)^{1/3}}{t} = \frac{M_{\text{oxide}} \cdot P_{\text{H}_2} \cdot k_o}{\rho_{\text{oxide}} \cdot r_0} \exp\left(-\frac{Q}{RT}\right) \quad [7]$$

Taking the logarithm on both sides of the Eq. [7] leads to the following relationship:

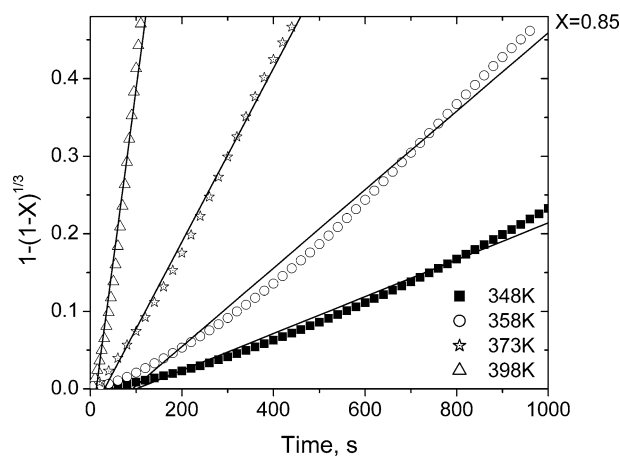


Fig. 8—Experimental values and theoretical linear fit corresponding to the chemical reaction rate for the isothermal reduction of Ag_2O .

$$\ln\left(\frac{1 - (1 - X)^{1/3}}{t}\right) = \ln\left(\frac{M_{\text{oxide}} \cdot P_{\text{H}_2} \cdot k_o}{\rho_{\text{oxide}} \cdot r_0}\right) - \frac{Q}{RT} \quad [8]$$

The plot of the term on the left-hand side against $1/T$ is presented in Figures 10 and 11 for Reactions [1] and [2], respectively. As can be seen in Figure 11, the experimental point corresponding to 923 K lies above the Arrhenius plot; this might suggest that above this temperature the reduction control is shifting due to the increase in temperature, *e.g.*, the faster the rate of chemical reaction is, the less likely to be the rate controlling mechanism. From the slopes of the Arrhenius plots, the activation energies for Reactions [1] and [2] are found to be 64 for Ag_2O and 124 kJ/mol for MoO_3 . According to Seetharaman *et al.*,^[16] the stronger the metal-oxygen bond, the higher the activation energy. In addition, the Mo-O bond is expected to be stronger,

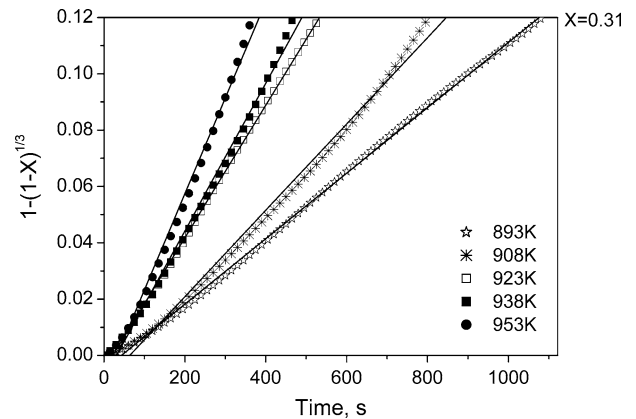


Fig. 9—Experimental values and theoretical linear fit corresponding to the chemical reaction rate for the isothermal reduction of MoO_3 .

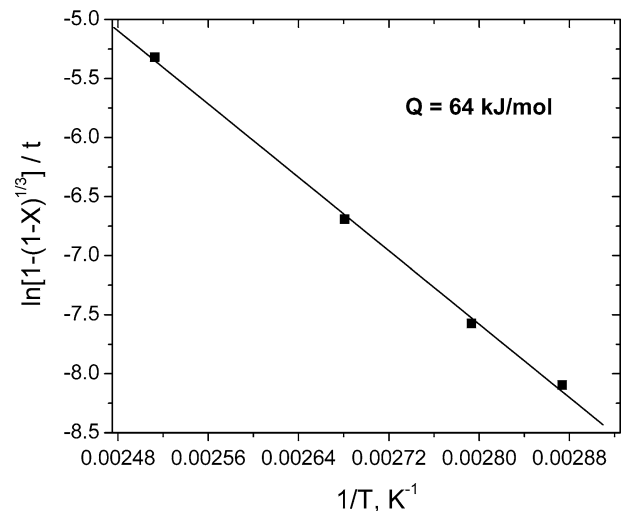


Fig. 10—Arrhenius plot for the isothermal reduction of Ag_2O .

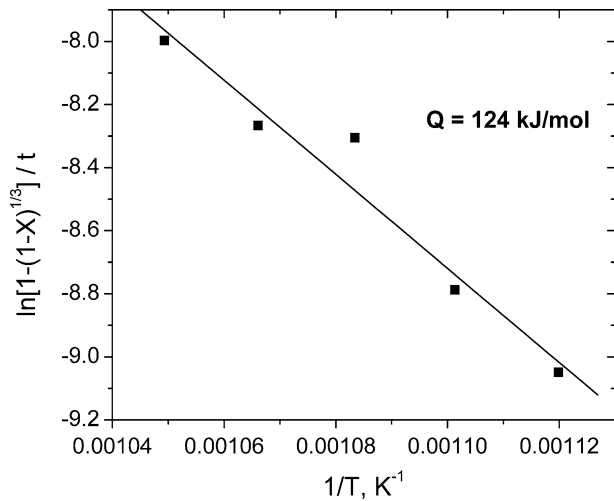


Fig. 11—Arrhenius plot for the isothermal reduction of MoO_3 .

because its free energy of formation has a larger negative value, which in turn counts for bond forces.

D. Nonisothermal Kinetic Analysis

For nonisothermal decomposition of carbonates, Arvanitidis *et al.*^[17,18] reported, on a shrinking core model, the activation energy for a chemical-reaction-controlled process. This approach would also be valid at the early stages of Reactions [4] and [2b] involved in the reduction of Ag_2MoO_4 . The mathematical expression for the reaction rate is

$$\frac{dX}{dt} = \frac{A_0}{R} \cdot \frac{(1-X)^{2/3}}{T} \cdot k \quad [9]$$

The new term, A_0 , is the initial reaction surface area. Inserting Eq. [6] into Eq. [9] leads to the following relationship:

$$\frac{dX}{dt} = \frac{A_0}{R} \cdot \frac{(1-X)^{2/3}}{T} \cdot k_o \exp\left(-\frac{Q}{RT}\right) \quad [10]$$

By taking the logarithm on both sides of Eq. [10] and rearranging the expression, one can obtain

$$\ln\left(\frac{dX}{dt}\right) + \ln(T) - \ln(1-X)^{2/3} = \ln B - \frac{Q}{RT} \quad [11]$$

where B groups $A_0 k_o / R$, which are independent of temperature. The three terms of the left-hand side of Eq. [11] can be obtained using the experimental data of Figure 7 taking the early stages of reduction for the regions corresponding to Reactions [4] and [2b]. Thus, plots using Eq. [11] for Reactions [4] and [2b] are presented in Figures 12 and 13, respectively. The value of the activation energy calculated from the slope in Figure 12 is 69 kJ/mol, which is in good agreement with the value obtained by isothermal experiments, 64 kJ/mol. It should be pointed out that, in Figure 12, the

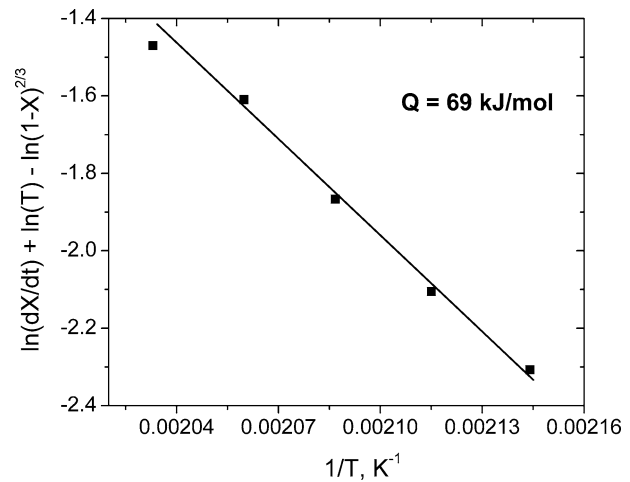


Fig. 12—Arrhenius plot for the nonisothermal reduction of Ag_2MoO_4 to Ag and MoO_3 .

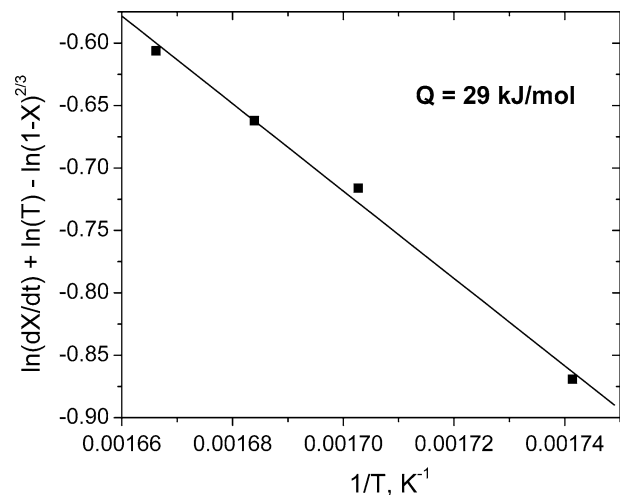


Fig. 13—Arrhenius plot for the nonisothermal reduction of MoO_3 to MoO_2 in the $\text{Ag}_2\text{O}-\text{MoO}_3$ system.

experimental point corresponding to the highest experimental temperature was left out of the calculations as it tends to deviate from the regression line. This deviation suggests that the thermal decomposition of Ag_2O (decomposition temperature of $\text{Ag}_2\text{O} \approx 473$ K) starts to play a mayor role in the reduction mechanism. The similarity of the activation energies obtained from both isothermal and nonisothermal temperature programs enables the possibility of predicting the kinetics of reactions from a single nonisothermal experiment. On the other hand, the activation energy of Reaction [2b] evaluated from the slope in Figure 13 is 29 kJ/mol. Because this value is significantly lower than that obtained from the isothermal experiments, *e.g.*, 124 kJ/mol, the assumption of silver lowering the activation energy of the proceeding reaction by catalysis appears to be valid. That is to say, in the reduction of

$\text{Ag}_2\text{O}\cdot\text{MoO}_3$, the strength of the Mo-O bond is likely to be weakened by the attraction of Ag to oxygen, which increases the reduction rate of MoO_3 to Mo. The present results suggest that the reduction process of Ag_2MoO_4 could be best achieved under nonisothermal conditions due to the low decomposition temperature of Ag_2O . In fact, the nonisothermal technique overcomes many limitations of the isotherm technique. For example, the nonisothermal technique represents a more realistic situation, because in most industrial reactors, the reacting materials are heated gradually. By the same token, no reactions take place isothermally, because all reactions are accompanied by a heat change, which is more significant when a large mass of materials react. On the other hand, the isothermal technique is inadequate to study complex reactions involving several series, parallel or overlapping reactions.

V. SUMMARY AND CONCLUSIONS

The reduction of Ag_2MoO_4 by hydrogen was studied by means of thermogravimetric technique under non-isothermal conditions. Previously, isothermal reduction experiments were performed on the individual oxides, viz. Ag_2O and MoO_3 . Nonisothermal results indicate that the reduction of Ag_2MoO_4 proceeds in three steps: one involving the reduction of Ag_2MoO_4 to silver and MoO_3 , a second step in which MoO_3 is reduced to MoO_2 , and the last step wherein MoO_2 is reduced to metallic molybdenum. From the rate of the reactions obtained, the activation energies for the two first steps were calculated to be 69 and 29 kJ/mol, respectively. The activation energy of the isothermal reduction of Ag_2O to Ag is in agreement with the first step of the nonisothermal experiment. On the other hand, the activation energy of the isothermal reduction of MoO_3 to MoO_2 , 124 kJ/mol, implies that the presence of silver in the second step of the nonisothermal reduction affects the reaction rate of MoO_3 to MoO_2 .

ACKNOWLEDGMENTS

The authors are thankful to Dr. Rafael Huirache for his valuable comments. Financial support from CONACYT, Mexico, for one of the authors (JCJ) is gratefully acknowledged.

REFERENCES

1. J.A. Bustnes, N.N. Viswanathan, Du Sichen, and S. Seetharaman: *Z. Metallkd.*, 2000, vol. 91, pp. 500–03.
2. J.A. Bustnes, N.N. Viswanathan, Du Sichen, and S. Seetharaman: *Metall. Mater. Trans. B*, 2000, vol. 31B, pp. 540–42.
3. D.T. Hawkins and W.L. Worrell: *Metall. Trans.*, 1970, vol. 1, pp. 271–73.
4. J. Orehotsky, L. Jamiolkowski, and J. Gerbec: *Mater. Sci. Eng.*, 1979, vol. 41, pp. 237–41.
5. J. Orehotsky and M. Kaczinski: *Mater. Sci. Eng.*, 1979, vol. 40, pp. 245–50.
6. P. Arnoldy, J.C.M. de Jonge, and J.A. Moulijn: *J. Phys. Chem.*, 1985, vol. 89, pp. 4517–26.
7. Du Sichen and S. Seetharaman: *Metall. Trans. B*, 1992, vol. 23B, pp. 317–24.
8. B.V. Lvov: *Thermochimica Acta*, 1999, vol. 333, pp. 13–19.
9. J. Stolk and A. Manthiram: *Metall. Mater. Trans. A*, 2000, vol. 31A, pp. 2396–98.
10. J. Bygdén, Du Sichen, and S. Seetharaman: *Metall. Mater. Trans. B*, 1994, vol. 25B, pp. 885–91.
11. W.V. Schulmeyer and H.M. Ortner: *Int. J. Refractory Met. Hard Mater.*, 2002, vol. 20, pp. 261–69.
12. T. Ressler, R.E. Jentoft, J. Wienold, M.M. Günter, and O. Timpe: *J. Phys. Chem. B*, 2000, vol. 204, pp. 6360–70.
13. J. Szekely, J.W. Evans, and Y.H. Sohn: *Gas-Solid Reactions*, Academic Press, New York, NY, 1976, p. 18.
14. O. Levenspiel: *Chemical Reaction Engineering*, John Wiley & Sons, New York, NY, 1962.
15. J.M. Smith: *Chemical Engineering Kinetics*, McGraw-Hill, New York, NY, 1981, pp. 643–47.
16. S. Seetharam, Du Sichen, and J.A. Bustnes: *Proc. Int. Symp. on Metallurgy and Materials of Non-Ferrous Materials and Alloys*, Northeastern University, Shenyang, China, 1996, pp. 669–75.
17. I. Arvanitidis, Du Sichen, and S. Seetharaman: *Metall. Mater. Trans. B*, 1996, vol. 27B, pp. 409–16.
18. I. Arvanitidis, Du Sichen, H.Y. Sohn, and S. Seetharaman: *Metall. Mater. Trans. B*, 1997, vol. 28B, pp. 1063–68.